Anisotropy field measurement in barium ferrite powders by applied field Mössbauer spectroscopy

Q A Pankhurst

Department of Physics, University of Liverpool, Liverpool L69 3BX, UK

Abstract. A new method for measuring magnetic anisotropy in ferrimagnetic powders using applied field Mössbauer spectroscopy has been developed. The method is based on using a uniaxial anisotropy mean-field model to calculate the equilibrium spin orientations as a function of applied field and compute the corresponding Mössbauer spectra. A variety of asymmetric broad line profiles are predicted which are sensitively dependent on the magnetization and the exchange and anisotropy terms. In principle the technique enables the determination of individual sublattice anisotropies, although in the case of pure and Co–Ti substituted barium ferrite the sublattice anisotropies are found to be experimentally indistinguishable. A mean anisotropy is obtained which compares favourably with the results of other measurements on barium ferrite.

1. Introduction

The hexagonal ferrite $BaFe_{12}O_{19}$ is potentially of great technological importance as a high density recording medium. Barium ferrite particles have a platelet morphology and an easy axis of magnetization which is normal to the plate, and as such are well suited to perpendicular recording. Barium ferrite media are oxidation and corrosion resistant, insensitive to pressure-induced demagnetization, and may be mass-produced using existing manufacturing technologies.

One disadvantage associated with $BaFe_{12}O_{19}$ is that it has a large intrinsic coercivity H_c resulting from the magnetic anisotropy of the material. This problem is usually overcome by substituting equimolar quantities of Co^{2+} and Ti^{4+} ions into the Fe^{3+} sites, which is found to reduce the coercivity to levels acceptable for magnetic recording without significantly affecting the magnetization [1].

The explanation of the reduced H_c in Co–Ti substituted barium ferrite lies in the nature of the magnetic anisotropy, which is uniaxial and results from two competing terms: a crystalline term and a shape anisotropy term. The crystalline anisotropy dominates and determines that the easy magnetization axis be along the hexagonal c axis (perpendicular to the plate), while the shape anisotropy opposes such an orientation. Ascribing the effective fields H_K and H_d to these anisotropies the coercivity may be expressed as

$$H_c = \alpha(H_K - H_d) \tag{1}$$

where α is a constant. Following the Stoner–Wohlfarth coherent rotation model for non-interacting particles [2], $\alpha = 1$ for perfect alignment of the easy axes, and 0.48 for a random assembly, and the anisotropy fields are

$$H_K = 2K/M_s \qquad H_d = (N_\parallel - N_\perp)M_s. \qquad (2)$$

Here K is the crystalline anisotropy constant, M_s is the saturation magnetization per unit volume, and $N_\parallel$ and $N_\perp$ are the demagnetising factors parallel and perpendicular to the easy axis. The effect of Co–Ti substitution into barium ferrite is both to reduce K and to increase $N_\parallel - N_\perp$, while keeping M_s relatively constant, thereby reducing H_c.

The increase in $N_\parallel - N_\perp$ is simply morphological. Co–Ti-doped ferrites prepared by the glass crystallization method [3] or by the hydrothermal method [4] have particle diameters that may be controlled in the range 100–5000Å with aspect ratios (diameter/thickness) in the range 2–10. The shape anisotropy is larger in platelets with larger aspect ratios [5].

The decrease in K with increasing Co–Ti content is well established [6,7] but is less well understood. It has been suggested that the largest contributions to K comes from the single-ion anisotropies of Fe^{3+} ions at two of the five distinct lattice sites available to the metallic cations, namely the 12k and 2b sites [8]. There is also evidence that the Co^{2+} and Ti^{4+} ions preferentially occupy one or the other or both of these sites [6,9–12]. The single-ion anisotropy of Co^{2+} ions at octahedral sites, such as 12k, has been shown to be negative, i.e. favouring orientations perpendicular to the c axis [13]. The net reduction in K may therefore be attributed to the negative contributions of the Co^{2+} ions and the zero contributions of the non-magnetic Ti^{4+} ions. An alternative explanation is that the Ti^{4+} ions preferentially occupy the 2b sites, resulting in non-magnetic layers perpendicular to the c axis, separating magnetic regions [14,15]. This may lead to incoherent magnetization rotation in an applied field, which would be observed experimentally as a reduction in K.

There are many experimental techniques for measuring the anisotropy field $H_A = H_K + H_d$. These include analysing the curve of magnetization as a function of applied field, comparing the work required to saturate the sample magnetization in different directions, measuring the torque produced by the applied field, and microwave ferrimagnetic resonance [16]. However, these methods rely on the availability of either single-crystal or highly oriented particulate samples. More recently some methods have been developed for use with powder samples. These include the rotational hysteresis loss [17], reversible transverse susceptibility [18], and d^2M/dH^2 singular-point detection [19] methods. One factor that all these techniques have in common is that the anisotropy that is measured is the sum of all the contributions from all the various lattice sites.

In this paper a new method of measuring anisotropy in ferrimagnetic powders is presented with which, in principle at least, it is possible to distinguish and determine the *individual sublattice anisotropies*. The method is based on computer analysis of the Mössbauer spectra of the powders in applied fields in terms of a suitably constructed spin Hamiltonian model. The work is an extension of a recent study of the Mössbauer spectra of antiferromagnetic powders in applied fields [20], in which it was shown that anisotropy fields could be reliably determined from such data.

In the following section the theoretical basis of the model is presented. Thereafter the technique is applied to both pure and Co–Ti substituted barium ferrite.

2. Method

The Hamiltonian for a uniaxial ferrimagnet subject to an external applied field H_{app} incorporates exchange, anisotropy and applied field terms :

$$\mathcal{H} = -2 \sum_{ij} J_{ij} S_i \cdot S_j - \sum_i K_i (S_{zi})^2 - g\mu_B \sum_i H \cdot S_i. \tag{3}$$

Here J_{ij} is the exchange constant between the ith and jth atoms, S_i and K_i are the spin and anisotropy of the ith atom, g is the spectroscopic splitting factor, and μ_B is the Bohr magneton. H is the local field at an atomic site, which in cgs units for the case of cubic symmetry is given by

$$H = H_{app} - N_{\parallel} M + \tfrac{4\pi}{3} M \tag{4}$$

where $N_{\parallel}$ is the demagnetization factor parallel to the easy axis $(0 \leq N_{\parallel} \leq 4\pi)$ and $\tfrac{4\pi}{3} M$ is the Lorentz cavity field.

As a starting point we consider a two-sublattice model in which nearest neighbour interactions dominate, with $J_{(i,j)} = J$ and $J < 0$ where (i, j) denotes a neighbouring pair of atoms. Writing the anisotropy constants of the two sublattices K and K', and the sublattice spins S and S', the Hamiltonian becomes

$$\mathcal{H} = -2J \sum_{(ij)} S_i \cdot S_j' - K \sum_i (S_{zi})^2 - K' \sum_j (S_{zj}')^2 - g\mu_B H \cdot \left(\sum_i S_i + \sum_j S_j' \right). \tag{5}$$

Using the mean-field approximation the energy of the system can be expressed in terms of the orientations of the sublattice spins:

$$E = NSg\mu_B [H_E \xi \cos(\theta - \theta') - \tfrac{1}{2} H_A \cos^2(\theta - t) - \tfrac{1}{2} H_A' \xi^2 \cos^2(\theta' - t) - H(\cos\theta + \xi\cos\theta')]. \tag{6}$$

Here N is the number of sublattice spins, and θ, θ' and t are the polar angles of the sublattice spins and the easy anisotropy axis with respect to the local field direction. ξ is the ratio of the spin magnitudes, S'/S. The exchange field $H_E = -2JzS/g\mu_B$ where z is the number of nearest neighbours, and the anisotropy fields are $H_A = 2KS/g\mu_B$ and $H_A' = 2K'S/g\mu_B$. Note that in this formalism K and K' are effective anisotropy constants which incorporate both crystalline and shape anisotropy terms.

For a given t the equilibrium spin configuration is obtained by solving the simultaneous equations $\partial E/\partial\theta = \partial E/\partial\theta' = 0$. In a powder the angle t is sampled continuously from 0 to 2π, with the range 0 to π encompassing all unique solutions. The Mössbauer spectrum of a powder is therefore a $\sin t$-weighted superposition of the subspectra corresponding to each value of t. It may be modelled by choosing a finite number (N_t) of representative values of t (e.g. $t = \cos^{-1}[(2n-1)/N_t]$, $n = 1, \ldots, N_t$) and calculating and summing the resulting subspectra. Values of $N_t \sim 20$ are usually large enough to give a good approximation (less than 1% error) while not exceeding computer resources.

To understand better the types of Mössbauer spectra this model gives rise to it is useful first to consider the range of equilibrium spin directions found by solving equation (6). If we choose an exchange field of 5000 kOe and local fields of up to 100 kOe the sublattice spins remain almost antiparallel throughout any reorientation;
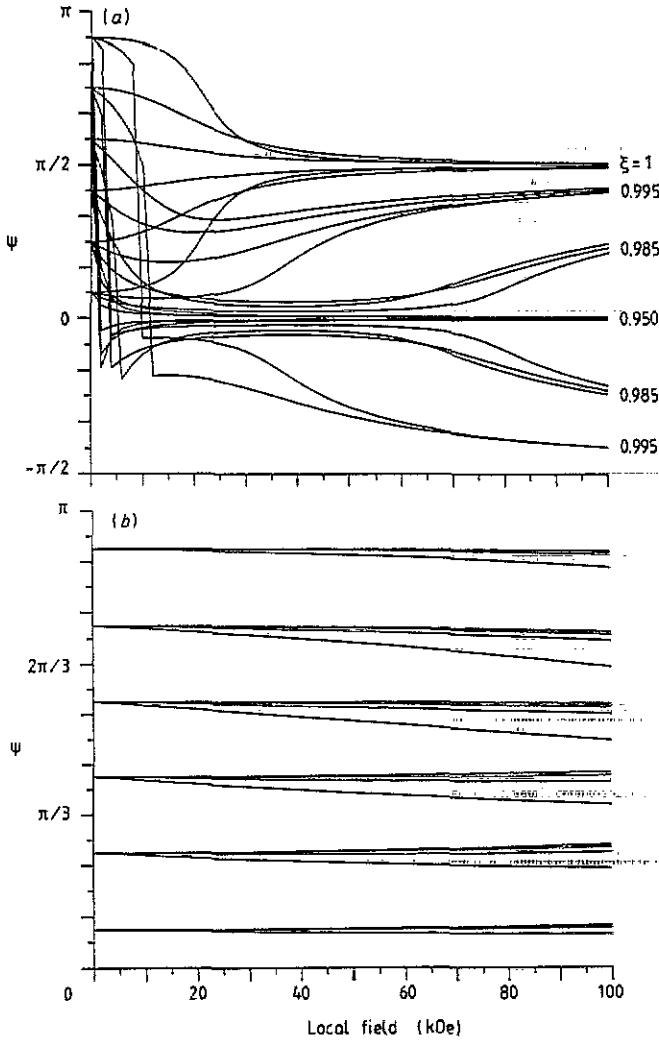
Figure 1. Variation as a function of local field H of the angle ψ between H and the antiferromagnetic axis of a two-sublattice uniaxial ferrimagnet with an exchange field $H_E = 5000$ kOe for sublattice spin ratios $\xi = 0.95$, 0.985, 0.995 and 1 and anisotropy fields (a) $H_A = 0.05$ kOe and (b) $H_A = 10$ kOe. Note the different abscissa scales. In (b) the uppermost curve in each branch has $\xi = 1$, the lowermost has $\xi = 0.95$.

the angle ψ between the antiferromagnetic axis of the spins and the local field is then approximately equal to θ and $\theta' - \pi$. In figure 1 ψ is plotted as a function of H for spin ratios $\xi = 1$, 0.995, 0.985 and 0.95, and for a variety of initial spin orientations $\psi_0 = \psi(H = 0)$ between 0 and π. For simplicity we take $H_A = H_A'$.

Figure 1(a) is for an extreme of small anisotropy, $H_A = 0.05$ kOe. In the antiferromagnet ($\xi = 1$) the spin-flop phase transition takes place at $H \simeq \sqrt{2H_E H_A} = 22$ kOe, above which ψ approaches $\frac{\pi}{2}$. In a relatively strong ferrimagnet ($\xi = 0.95$) ψ rapidly nears zero with increasing H as the ferromagnetic moment aligns parallel to H. The weaker ferrimagnets ($\xi = 0.985$ and 0.995) exhibit a mixture of antiferromagnet-like spin-flop behaviour and ferromagnet-like alignment behaviour—the former being ap-

parent at high fields and the latter producing sharp changes in ψ at $H \sim 10$ kOe for values of $\psi_0 > \pi/2$. Figure 1(b) shows the curves of $\psi(H)$ for a relatively large anisotropy, $H_A = 10$ kOe. In this case the spins are to a large extent fixed in space, and it is only the stronger ferrimagnet that shows any appreciable spin rotation. At intermediate values of H_A the corresponding plots of $\psi(H)$ become complex, but retain, to varying degrees, the features evident in figures 1(a) and 1(b).

Figure 2 shows the simulated ^{57}Fe Mössbauer spectra of a two-sublattice ferrimagnet with spin ratio $\xi = 0.95$. Parameters of relevance to high-spin Fe^{3+} compounds were assumed: linewidth $\Gamma = 0.26$ mm s^{-1}, hyperfine fields $H_{hf} = 500$ kOe and $H'_{hf} = 475$ kOe, exchange field $H_E = 5000$ kOe, and anisotropy fields $H_A = H'_A = 0.05$, 2.5, 4.0, 4.75, 5.0 and 10 kOe. For clarity the isomer shift δ and the quadrupole splitting Δ were both taken to be zero. For each value of H_A four spectra are simulated, for local fields $H = 0$, 30, 60 and 90 kOe. It was assumed that $\boldsymbol{H}$ was equal to $\boldsymbol{H}_{app}$ (spherical particles, $N_{\parallel} = 4\pi/3$) and that the experimental geometry was of the 'transverse drive' type, in which the γ-rays are perpendicular to $\boldsymbol{H}_{app}$.

In a magnetically split ^{57}Fe spectrum with negligible electric quadrupole interaction the relative intensities of the outer : middle : inner pairs of lines which constitute the sextet are given by

$$3(1 + \cos^2 \vartheta) \ : \ 4\sin^2 \vartheta \ : \ (1 + \cos^2 \vartheta) \tag{7}$$

where ϑ is the angle between the incident γ-ray and the effective field at the nucleus, $\boldsymbol{H}_{eff}$. Here $\boldsymbol{H}_{eff}$ is the vector sum of $\boldsymbol{H}$ and $\boldsymbol{H}_{hf}$, where the orientation of $\boldsymbol{H}_{hf}$ has been determined from the calculated atomic spin orientation. In the case of Fe^{3+} ions $\boldsymbol{H}_{hf}$ is dominated by the Fermi contact interaction and is antiparallel to the atomic spin.

In zero applied field $\boldsymbol{H}_{eff} = \boldsymbol{H}_{hf}$ and $\boldsymbol{H}'_{eff} = \boldsymbol{H}'_{hf}$ for the two sublattices, and there is an isotropic distribution of ϑ over a sphere, giving $\overline{\sin^2 \vartheta} = \frac{2}{3}$ and relative line intensities $\frac{12}{3} : \frac{8}{3} : \frac{4}{3}$, i.e. 3:2:1. The outermost lines of the total spectrum correspond to the larger effective field, H_{eff}.

In the weak anisotropy regime, $H_A = 0.05$ kOe, the spins are free to reorient in response to a non-zero applied field and align with their ferromagnetic component parallel to $\boldsymbol{H}_{app}$. Thus $\boldsymbol{S}$ becomes parallel to $\boldsymbol{H}_{app}$ and $\boldsymbol{S}'$ becomes antiparallel to $\boldsymbol{H}_{app}$. Consequently on the first sublattice $H_{eff} = H_{hf} - H_{app}$ and the corresponding sextet 'shrinks', while on the second sublattice $H'_{eff} = H'_{hf} + H_{app}$ and the corresponding sextet 'expands'. This is evident in figure 2(a) where for $H_{app} \neq 0$ the outermost lines of the total spectrum correspond to H'_{eff}. Another feature is that $\vartheta = \pi/2$ for all the spins and the intensity ratios become 3:4:1 for both sublattices.

In the strong anisotropy regime, $H_A = 10$ kOe, the spins are essentially fixed in space, irrespective of the applied field. The effective fields are therefore the vector sums of $\boldsymbol{H}_{app}$ and an isotropic spherical distribution of the $\boldsymbol{H}_{hf}$ and $\boldsymbol{H}'_{hf}$. On the first sublattice the majority of the effective fields are approximately perpendicular to $\boldsymbol{H}_{app}$, with magnitudes $\overline{H_{eff}} \sim \sqrt{H_{hf}^2 + H_{app}^2}$; relatively few are approximately parallel to $\boldsymbol{H}_{app}$, with $H_{eff}^{max} \sim H_{hf} + H_{app}$; and even fewer are approximately antiparallel to $\boldsymbol{H}_{app}$, with $H_{eff}^{min} \sim H_{hf} - H_{app}$. On the second sublattice H'_{hf} replaces H_{hf} in these equations. The spins which produce the $\overline{H_{eff}}$ contributions are distributed (approximately) over a disc perpendicular to $\boldsymbol{H}_{app}$; the incident γ-rays encounter this disc edge on, giving $\overline{\sin^2 \vartheta} = \frac{1}{2}$ and subspectral intensity ratios of $\frac{9}{2} : \frac{4}{2} : \frac{3}{2}$. The H_{eff}^{max}

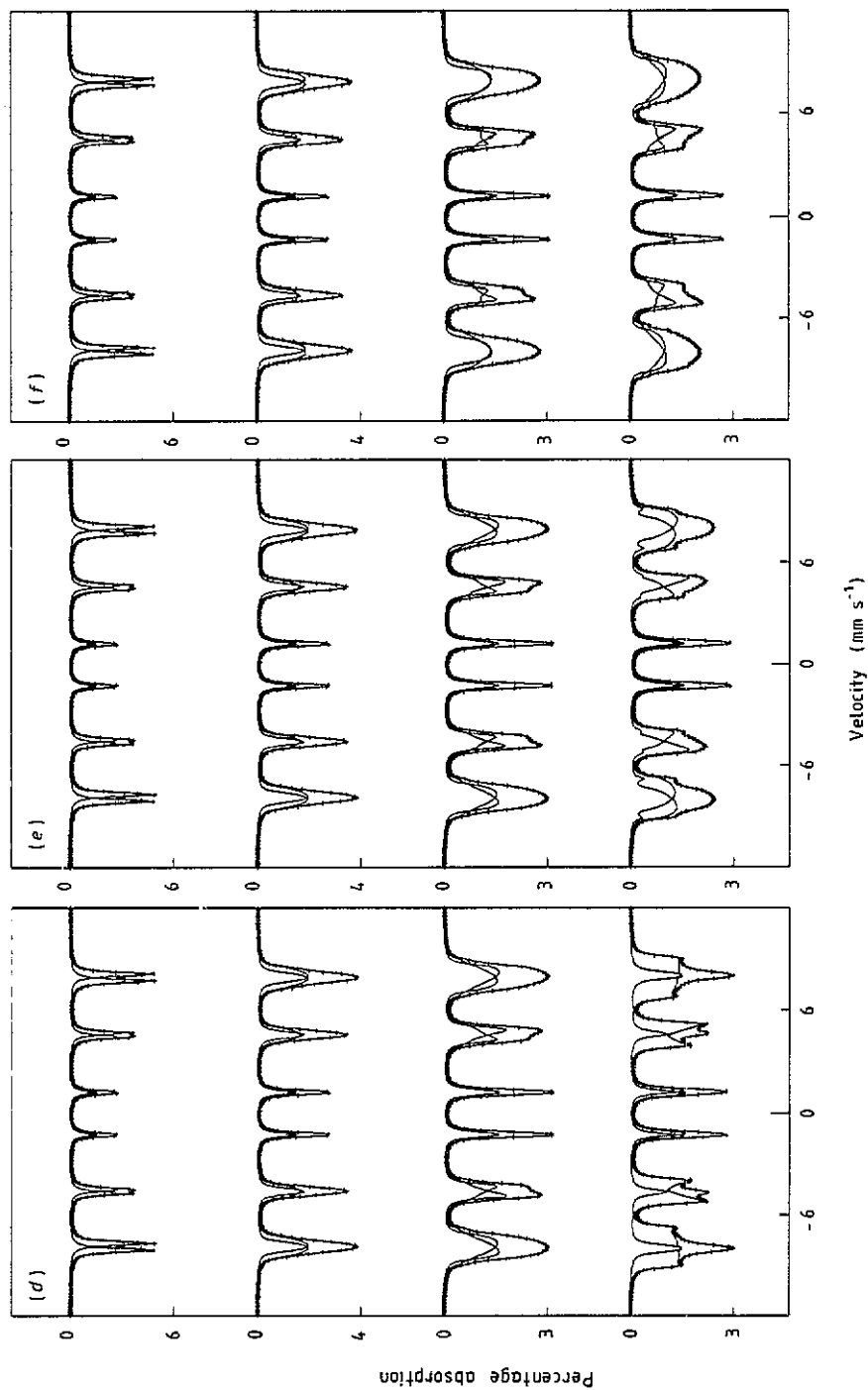Velocity (mm s^{-1})

Percentage absorption
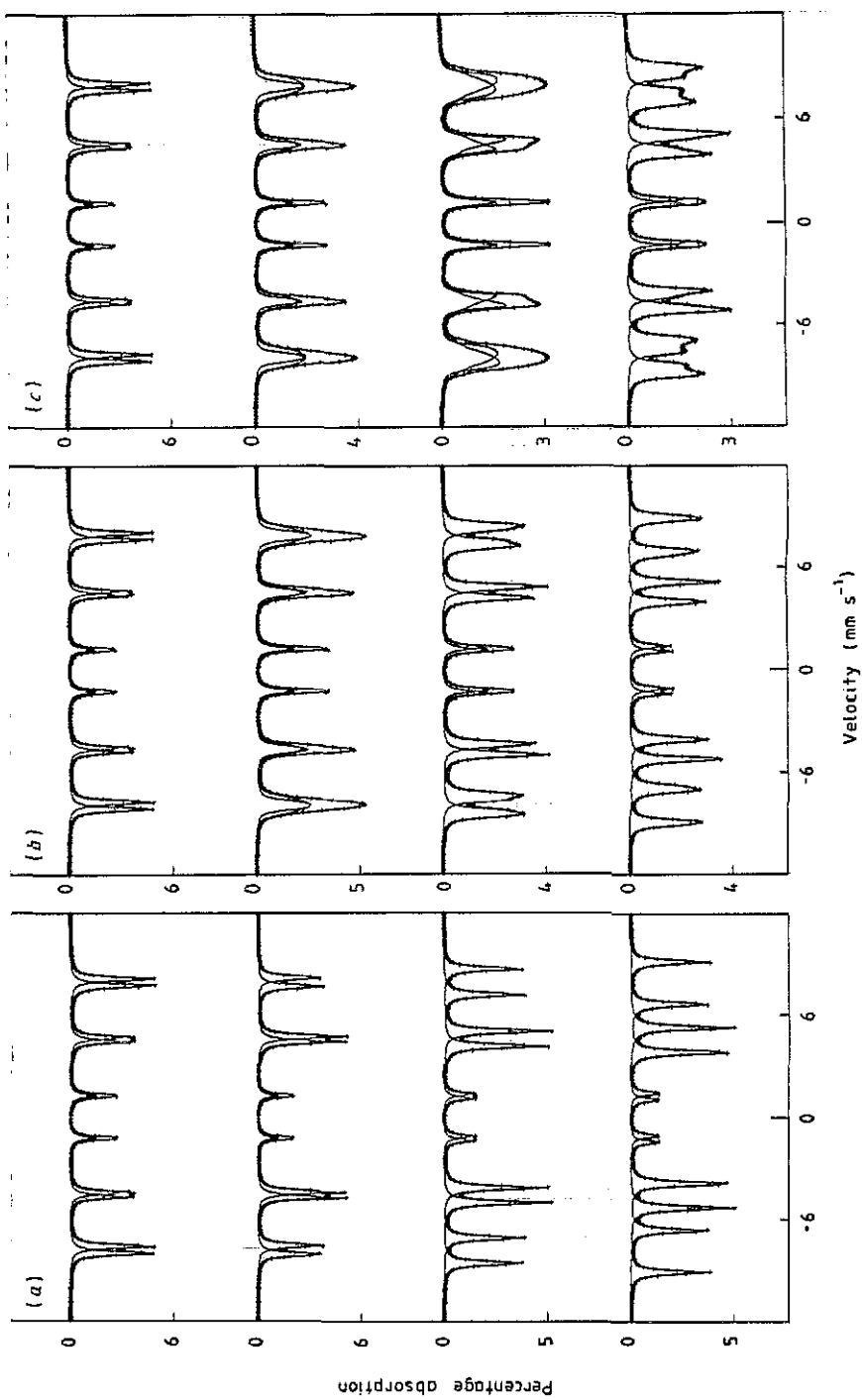
Figure 2. Simulated ^{57}Fe Mössbauer spectra of a two sublattice uniaxial ferrimagnetic powder with a sublattice spin ratio $\xi = 0.95$, exchange field $H_E = 5000$ kOe and hyperfine fields $H_{hf} = 500$ kOe and $H'_{hf} = 475$ kOe, subject to transverse applied fields of strength $H_{app} = 0, 30, 60$ and 90 kOe. Sets of spectra, (a)–(f), are shown for anisotropy fields $H_A = 0.05, 2.5, 4.0, 4.75, 5.0$ and 10 kOe.

and $H_{\text{eff}}^{\text{min}}$ spins make 3:4:1 contributions which are most readily apparent in the shapes of the second and fifth lines of the accumulated spectrum, as seen in figure 2(f).

At intermediate anisotropies, as in figures 2(b) to 2(e), the spectra gradually evolve from the sharp lineshapes of the weak anisotropy regime to the broad lineshapes of the strong anisotropy regime. It may be noted that for each non-zero applied field there is a 'cut-off' anisotropy field which, as far as the Mössbauer effect is concerned, is indistinguishable from infinity. For example, with $H_{\text{app}} = 30$ kOe the spectra with $H_A \geq 2.5$ kOe are very similar; the same applies for $H_{\text{app}} = 90$ kOe and $H_A \geq 4.0$ kOe. This implies that in cases of relatively high anisotropy large applied fields may be required to enable the measurement of H_A to be performed.

It should be noted that the simulations shown in figure 2 are intended only as an illustration of the diversity of the possible Mössbauer spectra of ferrimagnetic powders in applied fields. Different combinations of exchange, hyperfine and anisotropy field would produce substantially different spectra. Non-equivalent sublattice anisotropies could result in the mixing of significantly different subspectra—in an extreme case one might see a sharp line profile from one sublattice superimposed on a broad line profile from the other sublattice. The degree of ferrimagnetism, parametrized by the ratio of sublattice spins, would also have a profound effect on the observed spectra.

On a lesser scale, several other factors could influence the spectra. A non-zero electric quadrupole interaction would give rise to a 'quadrupole shift' of the inner four lines of a component sextet relative to the outer two lines; the magnitude of this shift would depend on the direction of H_{eff} with respect to the electric field gradient principal axis. A non-random distribution of crystallite orientations in the powder would induce a departure from the ideal intensity ratio of 3:2:1 in zero applied field, and would affect subsequent spectra. Finally, if the magnetic order was not saturated or if spin-wave fluctuations were significant the hyperfine field might vary as a function of applied field.

Despite these complications, the evolution from a characteristic sharp lineshape at weak anisotropy to a characteristic broad lineshape at strong anisotropy would remain, and as such it should still be possible to employ the applied field Mössbauer spectroscopy method to measure the anisotropy.

3. Experimental results

Two barium ferrite samples were selected for the Mössbauer experiments; their measured morphological and magnetic parameters are summarized in table 1. Both samples were manufactured using the hydrothermal method by Sakai Chemical Industries of Osaka, Japan. Transmission electron micrographs showed that the particles were nearly perfect hexagonal platelets of almost uniform dimensions. Mössbauer absorbers were prepared by mixing the powders with boron nitride and clamping between plastic discs.

Spectra were recorded at 4.2 K in the 'transverse drive' geometry, with applied fields of 0, 30, 60 and 90 kOe perpendicular to the γ-ray beam direction. These are shown in figures 3 and 4. Two features are immediately clear, the first being that there are a large number of lines, and so the spectra appear complex. This is because the Fe^{3+} ions at each of the five distinct lattice sites give different Mössbauer spectra. (The crystallographic and magnetic characteristics of the five sites are given in table 2.) Secondly, the line profiles are generally 'sharp', implying that in terms

Table 1. Morphological and magnetic parameters of the $BaFe_{12-2x}Co_xTi_xO_{19}$ samples studied [14]: diameter d (nm), diameter to thickness ratio d/t, specific surface area SSA (m^2 g^{-1}), room temperature saturation magnetization σ_s (emu g^{-1}) and coercivity parallel to the ferrimagnetic axis H_c (Oe).

Sample	d	d/t	SSA	σ_s	H_c
$x = 0$	330	2.5	25.8	72.2	2760
$x = 0.75$	110	7.0	30.5	52.8	605

of the Mössbauer methodology the samples are in the 'weak' anisotropy regime. The spectra of the Co–Ti substituted sample are somewhat broader than for the pure sample, but since this is true also for the zero-applied-field spectra the broadening is likely to be due to the substituents introducing some randomness into the local environments of the Fe^{3+} ions. This would result in a distribution in the hyperfine fields experienced by the Fe nuclei.

Table 2. Crystallographic and magnetic characteristics of the Fe^{3+} sites in the M-type hexagonal ferrite $BaFe_{12-2x}Co_xTi_xO_{19}$. The site occupancy of the Co–Ti substituted ferrite was determined from Mössbauer data recorded above and below the Curie temperature [12].

Sublattice	Coordination	Spin	Occupancy ($x = 0$)	Occupancy ($x = 0.75$)
12k	Octahedral	Up	12	10.2
$4f_{IV}$	Tetrahedral	Down	4	4
2a	Octahedral	Up	2	2
$4f_{VI}$	Octahedral	Down	4	3.4
2b	Five-fold	Up	2	1.4

As a first approximation the spectra were modelled using the two sublattice formulation described in the previous section. This is tantamount to assuming that in response to the applied field all the spins on the spin 'up' sublattices (12k, 2a and 2b) remain parallel to each other and all the spins on the 'down' sublattices ($4f_{IV}$ and $4f_{VI}$) remain parallel to each other, but that the 'up' and 'down' spins do not necessarily remain antiparallel to each other. Furthermore the anisotropies of all five sublattices were assumed to be the same, with $H_A = H'_A$. It was anticipated that if these approximations were too severe a significant misfit would be apparent in the fitted spectra.

The spin-ratio parameter ξ was determined by assuming that the hyperfine field at each lattice site was proportional to the spin of an atom on that site, so that

$$\xi = \left(\sum_i f_i H_{hf_i}\right) \Big/ \left(\sum_j f_j H_{hf_j}\right) \tag{8}$$

where f_i denotes the fractional occupancy of the spin 'down' sites and f_j refers to the spin 'up' sites. Similar assumptions have previously been found to be valid in calculations of the temperature dependence of the magnetization of barium ferrite [21]. The exchange field H_E was determined by deriving an expression relating it to the Curie temperature T_C. From mean field theory the free energy of the system may
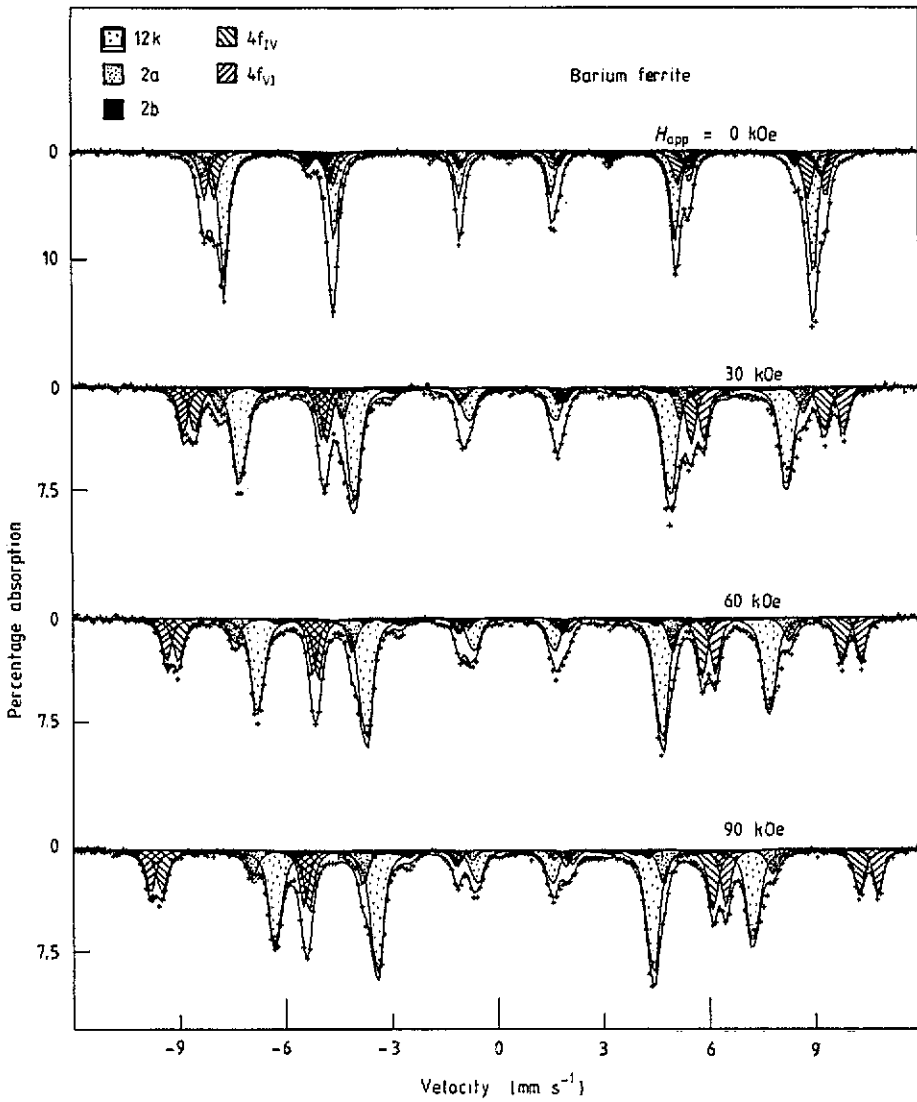
Figure 3. Spectra of BaFe$_{12}$O$_{19}$ at 4.2 K, transverse drive geometry. The full curves were obtained by simultaneously fitting all four spectra using the model described in the text.

be equated to the internal energy of the exchange field, and it can be shown that

$$T_C = \frac{4Jz}{3k_B} \frac{SS'}{(S^2 + S'^2)} \sqrt{S(S+1)S'(S'+1)}. \tag{9}$$

In an antiferromagnet $S' = S$ and equation (9) becomes the familiar equation $T_N = 2JzS(S+1)/3k_B$, where T_N is the Néel temperature.

Several other assumptions and approximations were made. The local field was taken to be equal to the applied field. The electric field gradient at each site was taken to be axially symmetric, and to have a principal axis parallel to the easy anisotropy axis. In each component sextet the linewidths of the middle and outer pairs of lines were allowed to be incrementally broader than the inner pair of lines, by amounts $\Delta\Gamma$
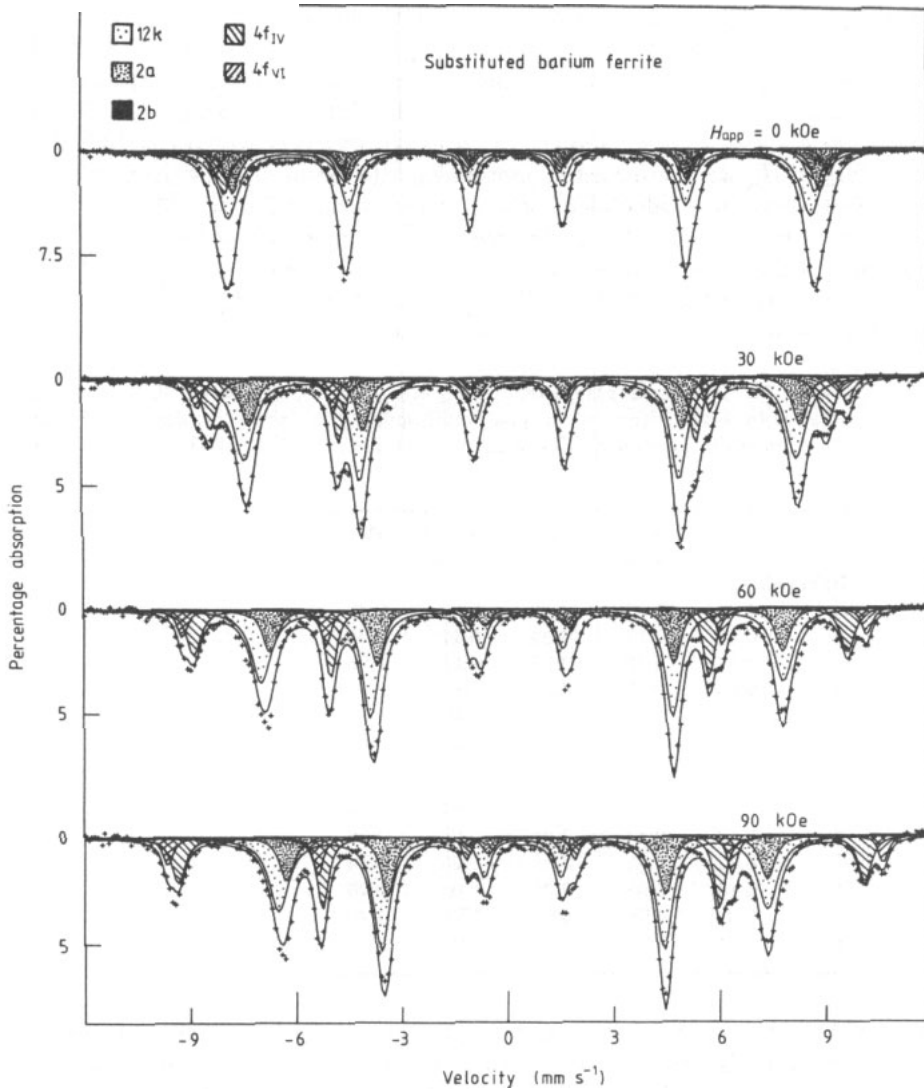
Figure 4. Spectra of $BaFe_{10.5}Co_{0.75}Ti_{0.75}O_{19}$ at 4.2 K, transverse drive geometry. The full curves were obtained by simultaneously fitting all four spectra.

and $2\Delta\Gamma$ respectively, as a means of taking into account sample inhomogeneity. The hyperfine fields were not strictly required to be independent of the applied field. The occupancy of the Fe^{3+} sites in each sample were taken to be those listed in table 2, as previously determined from Mössbauer data recorded above and below the respective Curie temperatures [12]. Lastly, it was assumed that the spin 'up' spins were of magnitude $S = \frac{5}{2}$.

For each sample all four spectra, with $H_{app} = 0$, 30, 60 and 90 kOe, were simultaneously least-squares fitted. Simultaneous fitting alleviates the problems associated with the interdependence of the fit parameters. Since H_E and H_A have no effect on the zero-applied-field spectrum a good fit of that spectrum determines the parameters δ, Δ, Γ, $\Delta\Gamma$ and H_{hf}. Equation (8) may then be used to calculate ξ from the H_{hf}

values, and equation (9) used to estimate H_E using the known Curie temperatures of the samples ($BaFe_{12}O_{19}$ has $T_c \simeq 723$ K, $BaFe_{10.5}Co_{0.75}Ti_{0.75}O_{19}$ has $T_C \simeq 590$ K [15]). This leaves H_A as the only free parameter used to fit the $H_{app} \neq 0$ spectra.

The fitted parameters are given in table 3. For the $BaFe_{12}O_{19}$ sample the fit gave $\xi = 0.53$ and so $H_E = 9520$ kOe, and the fitted anisotropy field was $H_A = 10.7$ kOe. The uncertainty in H_A was estimated by monitoring the goodness-of-fit parameter χ^2. A 68% confidence level was calculated for a χ^2 distribution with $\nu = 2000$ degrees of freedom [22]; this corresponded to an increase in χ^2 of order 1.5% with respect to its optimum value. This in turn translated into the confidence limits $9.4 \leq H_A \leq 11.9$ kOe. For the Co–Ti substituted sample $\xi = 0.57$, $H_E = 6980$ kOe and $H_A = 12.5$ kOe were obtained, with confidence limits $11.1 \leq H_A \leq 14.0$ kOe.

Table 3. Mössbauer parameters of $BaFe_{12-2x}Co_xTi_xO_{19}$ at 4.2 K: isomer shift relative to α-iron δ (mm s^{-1}), quadrupole splitting Δ (mm s^{-1}), linewidth Γ (mm s^{-1}), linewidth increment $\Delta\Gamma$ (mm s^{-1}), hyperfine field H_{hf} (kOe) and relative area RA.

	12k	4f$_{IV}$	2a	4f$_{VI}$	2b
$BaFe_{12}O_{19}$					
δ	0.46	0.37	0.42	0.48	0.42
Δ	0.40	0.17	0.04	0.17	2.34
Γ	0.27	0.26	0.26	0.26	0.26
$\Delta\Gamma$	0.02	0.01	0.04	0.01	0.01
H_{hf}	518	523	539	547	427
RA	48.2	18.7	10.7	16.5	6.0
$BaFe_{10.5}Co_{0.75}Ti_{0.75}O_{19}$					
δ	0.43	0.37	0.53	0.49	0.48
Δ	0.06	0.14	0.21	0.08	2.79
Γ	0.32	0.29	0.35	0.29	0.40
$\Delta\Gamma$	0.13	0.08	0.03	0.03	0.25
H_{hf}	511	518	516	539	410
RA	49.1	20.1	16.3	9.2	5.4

The overall quality of the fits is good, implying that the two-sublattice, single-anisotropy-field model is sufficient to describe the applied field response of barium ferrite. The potential for resolving sublattice anisotropies has therefore not been realized. This may be attributed to the strong degree of ferrimagnetism in the materials, compared to which the anisotropy becomes relatively insignificant in the presence of an applied field.

At first sight the fitted anisotropy fields of the two samples, 10.7 and 12.5 kOe, are surprisingly close in magnitude, considering that the room temperature coercivities are of order 2.8 and 0.6 kOe respectively. However, rotational hysteresis loss measurements of the temperature dependence of H_A in very similar samples have shown quite different behaviour in the pure and substituted materials [15]. In a pure sample with a slightly larger aspect ratio, $d/t = 4$, H_A was found to decrease from 10.0 kOe at room temperature to 9.8 kOe at 100 K, with a minimum of 9.3 kOe at about 190 K. In a $BaFe_{12-2x}Co_xTi_xO_{19}$ sample with $x = 0.58$ and the same aspect ratio as the $x = 0.75$ sample used in this work H_A was found to increase smoothly from 5.4 kOe at room temperature to 7.8 kOe at 100 K. Should these trends continue it is quite plausible that at 4.2 K the anisotropy field in the substituted ferrite might exceed that in the

pure sample.

It is also noticeable that the outermost lines of the zero-applied-field spectra move outwards as the external field increases; this appears to contradict the simulations shown in figure 2. The explanation of this is evident from the hyperfine field values in table 3: the outermost lines, with largest H_{hf}, correspond to the spin 'down' sites $4f_{IV}$ and $4f_{VI}$. They therefore correspond to the effective spin S'. In the simulations of figure 2 the outermost lines at $H_{app} = 0$ corresponded to the larger spin, S.

4. Conclusions

A methodology for using applied field Mössbauer spectroscopy to determine the anisotropy of ferrimagnetic powders has been developed. The technique has the potential advantage of permitting the resolution of sublattice anisotropies. This potential was not realized in the case of barium ferrite, although a mean anisotropy field was measured that compares favourably with the results of measurements made using other techniques. The method therefore appears to be reliable and has a good potential for future application. Work is currently in progress with several other ferrimagnets, including γ-Fe_2O_3. Consideration is also being given to a possible increase in resolution offered by directing the Mössbauer γ-ray beam parallel to the applied field direction.

References

[1] Kubo O, Ido T and Yokoyama H 1982 *IEEE Trans. Magn.* **MAG-18** 1122–4
[2] Stoner E C and Wohlfarth E P 1948 *Phil. Trans. R. Soc.* A **240** 599–642
[3] Kubo O, Ido T, Yokoyama H and Koike Y 1985 *J. Appl. Phys.* **57** 4280–2
[4] Barb D, Diamandescu L, Rusi A, Tărăbăsanu-Mihăilă D, Morariu M and Teodorescu V 1986 *J. Mater. Sci.* **21** 1118–22
[5] Osborn J A 1945 *Phys. Rev.* **67** 351–7
[6] De Bitetto D J 1964 *J. Appl. Phys.* **35** 3482–7
[7] Turilli G and Paoluzi A 1988 *IEEE Trans. Magn.* **MAG-24** 2865–7
[8] Asti G and Rinaldi S 1976 *Proc. Joint MMM–Intermag Conf. (Pittsburgh)* ed J J Becker and G H Lander (New York: American Institute of Physics) pp 214–6
[9] Casimir H B G, Smit J, Enz U, Fast J F, Wijn H P J, Gorter E W, Duyvesteyn A J W, Fast J D and de Jong J J 1959 *J. Physique Radium* **20** 360–73
[10] Belov V F, Khimich T A, Shipko M N, Zheludev I S, Korneev E V and Ovanesyan N S 1973 *Sov. Phys.-JETP* **35** 1089–95
[11] Yamada H, Takano M, Kiyama M, Takada T, Shinjo T and Watanabe K 1986 *Advances in Ceramics* vol 16, ed F F Y Wang (Columbus, OH: American Ceramics Society) pp 169–73
[12] Pankhurst Q A, Jones D H, Morrish A H, Zhou X Z and Corradi A R 1989 *Proc. 5th Int. Conf. on Ferrites (Bombay)* vol 1, ed C M Srivastava and M J Patni (Bombay: Oxford and IBH Publishing) pp 323–7
[13] Lotgering F K, Enz U and Smit J 1966 *Philips Res. Rep.* **16** 441–54
[14] Corradi A R, Speliotis D E, Morrish A H, Pankhurst Q A, Zhou X Z, Bottoni G, Candolfo D, Cecchetti A and Masoli F 1988 *IEEE Trans. Magn.* **MAG-24** 2862–4
[15] Corradi A R, Speliotis D E, Bottoni G, Candolfo D, Cecchetti A and Masoli F 1989 *IEEE Trans. Magn.* **MAG-25** 4066–8
[16] See e.g. Morrish A H 1965 *The Physical Principles of Magnetism* (New York: Wiley) pp 316–8
[17] Paige D M, Hoon S R, Tanner B K and O'Grady K 1984 *IEEE Trans. Magn.* **MAG-20** 1852–4
[18] Pareti L and Turilli G 1987 *J. Appl. Phys.* **61** 5098–101
[19] Scholl R, Elk K and Jahn L 1989 *J. Magn. Magn. Mater.* **82** 235–8
[20] Pankhurst Q A and Pollard R J 1990 *J. Phys.: Condens. Matter* **2** 7329–37
[21] van Wieringen J S 1967 *Philips Tech. Rev.* **28** 33–43
[22] Press W H, Flannery B P, Teukolsky S A and Vetterling W T 1986 *Numerical Recipes* (Cambridge: Cambridge University Press) ch 14